Materials and Design 193 (2020) 108869

Contents lists available at ScienceDirect

Materials and Design

journal homepage: www.elsevier.com/locate/matdes

Innovative processing route combining fused deposition modelling and laser writing for the manufacturing of multifunctional polyamide/carbon fiber composites

Federico Lupone [a], Elisa Padovano [a,*], Antonino Veca [b], Lorena Franceschetti [a], Claudio Badini [a]

[a] Politecnico di Torino, Department of Applied Science and Technology, Corso Duca degli Abruzzi 24, 10129 Torino, Italy.
[b] C.R.F. S.C.p.A. – Group Materials Labs, C.so Settembrini 40, Torino 10135, Italy

HIGHLIGHTS

- An innovative manufacturing route combining fused deposition modelling and laser writing was successfully developed.
- Laser writing was performed on FDM samples to obtain "in situ" conductive tracks on their surface.
- Tensile properties and track resistance of FDM specimens were correlated to the fiber orientation inside the layers.
- The lowest electrical resistance values ever reached by laser writing on metal free polymer composites were obtained.

GRAPHICAL ABSTRACT

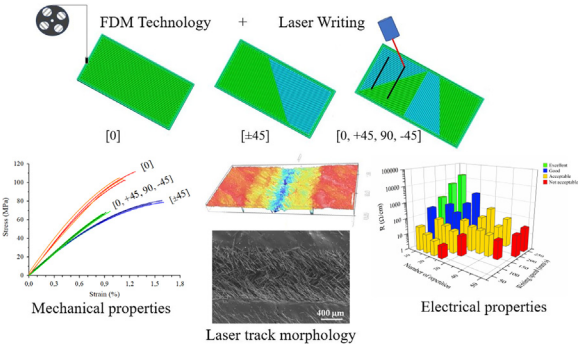

ARTICLE INFO

Article history:
Received 4 February 2020
Received in revised form 5 June 2020
Accepted 6 June 2020
Available online 8 June 2020

Keywords:
Fused deposition modelling
Polymer-matrix composites
Carbon fibers
Electrical properties
Laser processing

ABSTRACT

An innovative manufacturing method, based on Fused Deposition Modelling (FDM) and Laser Writing (LW) technologies, was developed to integrate electrically conductive tracks within high strength 3D printed parts. Carbon fibers reinforced polyamide composites were processed by FDM according to three different printing architectures by varying the raster angle in the layer sequence. Laser writing was then performed to obtain conductive tracks on the surface of the printed parts. The process-structure-property relationship of components before and after the writing of conductive tracks was investigated. The tensile behaviour and the track resistance of samples were correlated to the direction of filament extrusion within the layers, and consequently to fibers orientation. Tracks showing good aesthetic quality and the lowest electrical resistance were obtained on samples with [±45] architecture. These tracks displayed the lowest electrical resistance ever reached by laser writing on metal-free polymer composites (0.008 kΩ/cm). Samples with [±45] architecture also showed high strength (72.9 MPa) and stiffness (7.7 GPa). The integration of FDM and LW emerges as a new approach to transform the surface of high strength polymer composites parts into a highly valuable system. These multifunctional components can find applications in several industrial fields such as automotive, aeronautics, and appliances.

1. Introduction

In recent years, the integration of electrical circuits into polymers has attracted growing interest of both scientific and industrial communities because of its huge potential in several technological applications.

* Corresponding author.
E-mail addresses: federico.lupone@polito.it (F. Lupone), elisa.padovano@polito.it (E. Padovano), antonino.veca@crf.it (A. Veca), lorena.franceschetti@studenti.polito.it (L. Franceschetti), claudio.badini@polito.it (C. Badini).

https://doi.org/10.1016/j.matdes.2020.108869

Moreover, smart, highly customizable and easily recyclable products are increasingly required by industries, in compliance with stakeholder inputs. The combination of Additive Manufacturing (AM) technologies and laser processing, such as laser writing (LW), could be a new manufacturing approach able to face these challenges. In fact, laser systems find many industrial applications thanks to their high speed, precision and energy-efficiency. On the other hand, AM has emerged as one of the most rapidly growing research topics in both academia and industry, and it is rapidly changing from a rapid prototyping technology to an established method for manufacturing end-use products [1].

The additive principle, based on a layer-by-layer manufacturing strategy, offers an unprecedented design freedom and allows to produce complex shapes without the use of tools and moulds, thus reducing the time-to-market of new products [1]. In recent years, great efforts have been made to expand the material palette to be processed by AM technologies. In this frame, Carbon Fiber Reinforced Polymers (CFRPs) have attracted increasing attention due to the combination of their mechanical, electrical and thermal properties. Fused deposition modelling (FDM), which is one of the most popular AM techniques for the fabrication of plastic parts, is suitable for processing these composites. Moreover, it offers many advantages such as low-cost, high speed and simplicity [2].

The use of fiber reinforcement in FDM filaments has been widely investigated in the literature; many studies mainly focused the attention on the development of short fibers composites [2]. Carneiro et al. [3] studied glass fiber reinforced polypropylene composites and reported an increase of 30% and 40% of elastic modulus and strength respectively compared to pure polymer. Ning et al. [4] investigated the effect of carbon fibers (CF) on FDM build CF/ABS parts. The highest tensile strength and Young's modulus were obtained with 5 wt.% and 7.5 wt.% of carbon fibers respectively; higher loadings negatively affected the performance of the material due to higher void formation.

Brenken et al. [5] reviewed the FDM process of discontinuous fiber reinforced polymers and compared the mechanical properties of different composite material systems. The addition of carbon fibers to ABS or PLA increases both their tensile strength and Young's modulus. Generally, strength values ranging between 30 MPa and 70 MPa can be achieved when the applied load is parallel to the printing direction.

Several studied reported that the mechanical properties of FDM parts greatly depend on the adopted process parameters, particularly raster angle and building orientation [6–9]. This effect is more pronounced in 3D printed fiber reinforced composites due to the alignment of fibers along the printing direction; the biggest improvement of mechanical performances is observed when tensile loading direction is parallel to the extruded beads [2,5].

Tekinalp et al. [10] studied the influence of fiber orientation and porosity on the mechanical properties of 3D printed CF/ABS parts. These composited show very high fiber orientation in the printing direction (up to 91.5%) as a result of the high shear stresses inside the printer nozzle. The preferential alignment of fibers compensates the negative effect of porosity: an increase of 115% and 700% in tensile strength and Young's modulus was reported for 30 wt.% CF/ABS composites. Jiang et al. [11] investigated the effect on beads orientations on ABS, PLA and PETG reinforced with chopped carbon fibers and reported the highest tensile modulus and strength at 0° printing orientation. Liao et al. [12] observed a significant improvement of mechanical properties and thermal conductivity in CF/PA12 composites compared to the unfilled polymer. These results are explained by the uniform dispersion and preferential orientation of fibers along the extruded beads direction. Similar observations were carried out on several carbon fiber reinforced polymers processed by FDM [13–16].

Recently, high performance polymers, such as PPS [5], PEEK [17] and PEI [18], were also investigated for producing CFRPs through additive manufacturing. Moreover, co-extrusion and dual-nozzle FDM systems have been successfully introduced to manufacture continuous fiber reinforced composites, offering great improvement of mechanical properties compared to discontinuous fibers ones [19–21].

However, current applications of polymer composites, such as embedded sensing systems, frequently require multifunctional properties such as high specific strength and conductivity along selected directions [1]. Although conventional composites manufacturing processes are able to align conductive fillers within the polymer matrix, the electrical signal can pass through the entire material only in one direction [22]. To overcome this limit several methods have been developed to produce printed circuits on polymers surface, such as laser direct structuring, screen printing, inkjet printing and direct writing. Among them, electric functionalization of polymer composites via laser writing offers the possibility to create metal-free conductive tracks directly embedded in an insulating material. In fact, during laser writing a space resolved conductive path is produced within the irradiated lines. The laser exposure induces the pyrolysis of the polymer matrix. This leads to a local increase of the filler content over the percolation threshold within the track, thus retaining the insulating behaviour of the entire part [23–25]. Therefore, this technology shows important advantages in terms of process simplicity, resource efficiency and environmental impact over competing techniques. Laser writing prevents the use of copper wirings or conductive inks for electrical transmission, which are expensive and difficult to recycle. Therefore, it enables the design of smart components in a sustainable way and greatly simplifies their end-of-life disposal [26].

The use of laser writing to create conductive tracks was firstly described in a patent [23]; track resistance in the range from 0.9 to 1.3 kΩ/cm on carbon nanotubes (CNT)/polyethylene composites were reported. Liebscher et al. [25] found track resistances as low as 1.5 kΩ/cm in injection moulded CNT/PP/PC composites. Colucci et al. [26] reported low values of resistance in 2 wt.% CNT/PP composites (<1 kΩ/cm). However, the authors stated that a compromise between electrical properties and material integrity is required. Lastly, Caradonna et al. [27,28] studied several filler/polymer systems processed through different technologies. A systematic optimization of the laser writing parameters through a DOE approach allowed to obtain tracks with resistances of 0.02 kΩ/cm in CNT/PP/PC composites. However, to the best of our knowledge, no studies have been performed on laser functionalization of polymers reinforced with carbon fibers and processed by additive manufacturing.

The present paper deals with the laser writing of conductive tracks on a carbon fiber/polyamide composite manufactured by fused deposition modelling. The main objective of the research was to develop an innovative method to address the challenge of integrating electrical circuits within 3D printed parts, combining the advantages of both processes. For this purpose, a complete investigation was carried out to evaluate the microstructure and mechanical performance of 3D printed parts and to assess the influence of FDM and LW process parameters on the resulting electrical and morphological properties of the tracks. Because of several requirements have to be fulfilled for the industrial application of laser writing technology; the following guidelines are defined:

- The electrical resistance per length unit inside the tracks must be lower than 1 kΩ/cm.
- Very high resistance between not in contact adjacent tracks is required (i.e. at least four orders of magnitude higher than track resistance).
- Good aesthetic quality, which means no morphological defects and absence of deformation after laser processing, is needed.

2. Materials and methods

The experimental methodology used in this work consisted of three steps: characterization of the filament; investigation of microstructure

and mechanical properties of FDM printed parts; optimization of laser writing process parameters in terms of electrical behaviour and aesthetic quality of the tracks.

2.1. Material processing

A filament of polyamide reinforced with short carbon fibers (commercial name "Carbon PA", diameter of 1.75 mm) was purchased from Roboze SpA (Bari, Italy). According to the supplier, the material is specifically designed for the production of industrial components through FDM. The filament was printed using a Roboze One FDM printer (Roboze SpA, Bari, Italy), which was equipped with a 0.60 mm diameter stainless steel nozzle in order to avoid nozzle clogging and damage due to the abrasiveness of carbon fiber (Fig. 1A).

Dog-bone samples and rectangular plates were built-up in the xy plane, using three printing architectures (Fig. 1B), which differ in terms of bead orientation (i.e. raster angle) within the stacked layers. All samples were fabricated according to the printing parameters recommended by Roboze, that are reported in Table 1. A raft was used to improve bed adhesion and avoid warping. Dog-bone specimens were produced for microstructural and mechanical characterization according to ISO 527-4 standard (specimens of type 1B), while rectangular plates ($100 \times 100 \times 3$ mm^3) were used to perform laser writing treatment and evaluate the electrical properties of the tracks.

[0], [±45] and [0, 45, 90, −45].

Laser writing was carried out by a Towermark XL machine (Lasit, Italy), equipped with a pulsed CO_2 laser emitting in IR range (10.6 μm wavelength, maximum power of 100 W), scanning heads and focusing optics. The treatments were performed under N_2 atmosphere to avoid polymer oxidation. The surface of the tracks was gently cleaned with a jet of compressed air to eliminate carbonaceous residues and detached fibers. Plates produced with different raster angles (Fig. 1B) were treated with the same process parameters in order to identify the printing architecture that grants the best electrical properties of the tracks. The selected architecture was then adopted for the optimization of laser writing process parameters. To this purpose, parallel tracks were produced by changing the laser power (P) as percentage of the maximum power, the writing speed (v) and the number of repetitions (N). Frequency and defocusing were not considered because previous works showed that they did not influence the final properties of the tracks [27,28]. The repeatability of process was evaluated though the measurement of the electrical resistance of tracks produced on different plates. Moreover, the influence of track length (3, 6 and 9 cm) was also assessed. Laser writing was also performed on plates produced by injection moulding in order to compare the effect of laser functionalization on parts manufactured though different processing technologies. Carbon PA material including pristine filament and scraps from FDM plates (i.e. raft used to improve the adhesion of the first layers of component to the building plate) by using a EuroLab 16 mm XL twin-screw extruder

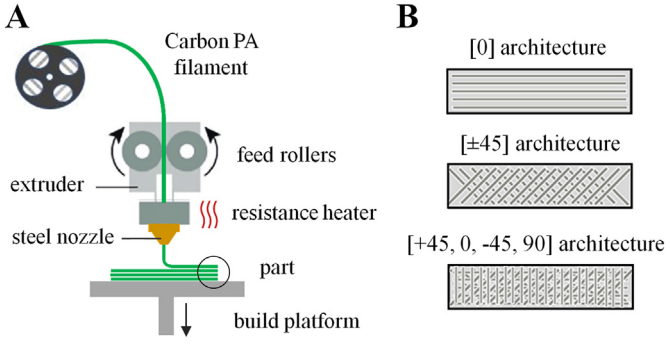

Fig. 1. (A) Conceptual sketch of the FDM manufacturing process and (B) schematic representation of 3D-printed specimens with different printing architectures:

Table 1
Process parameters used for carbon PA 3D printing.

T_{nozzle} (°C)	T_{bed} (°C)	Infill speed (mm/min)	Layer height (mm)	Object infill	Raster angle used in printing architectures (°)
300	45	3000	0.20	100%	[0], [±45], [+45, 0, −45, 90]

(Thermo Fisher Scientific, Waltham, MA, USA) with 40:1 L/D ratio and a final pelletizing unit. Rectangular plates with dimensions of $100 \times 100 \times 3$ mm^3 were then fabricated through a Babyplast 6/10P micro injection moulding machine (Cronoplast ST, Barcelona, Spain) with parameters shown as below: melting temperature of 280 °C, injection time of 10 s at 90 bar and total time cycle equals to 20 s. Laser writing was finally carried out on injection moulded plates using the process parameters previously optimized for 3D printed samples.

2.2. Characterization techniques

The thermal properties of the filament were investigated using a PerkinElmer Pyris 1 differential scanning calorimeter (PerkinElmer Inc., Waltham, MA, USA). The sample was tested with a heating-cooling cycle in the temperature range from 25 °C to 250 °C at a rate of 10 °C/min under nitrogen flow (50 mL/min). The glass transition, melting and crystallization temperatures and the crystalline fraction of the polymer matrix were evaluated. The crystalline fraction X_C was calculated according to Eq. (1):

$$X_C = \frac{\Delta H_m}{\Delta H_m^0 (1-f)} 100\% \quad (1)$$

where ΔH_m is the melting enthalpy, ΔH_m^0 is the melting enthalpy of fully crystalline PA6, equals to 240 J/g [29]), and f is the weight fraction of filler.

Thermal gravimetric analysis (TGA) was performed with a Mettler-Toledo TGA/SDTA 851e instrument in order to evaluate the thermal stability and the fiber content of the filaments. The temperature profile used in the experiment consisted of a complex thermal cycle based on the modified ISO 9924-3 standard [30]. The first part of the experiment was carried out in argon atmosphere and consisted of heating the sample from 25 °C to 600 °C at a rate of 10 °C/min, followed by a cooling step to 400 °C and staying at this temperature for 2 min. The sample was then heated in air from 400 °C to 800 °C with a rate of 10 °C/min; the maximum temperature was finally maintained for 20 min.

In order to investigate the carbon fiber length distribution, the filament was treated in a (Elite Thermal System Limited BSF 11/22, Italy) at 800 °C in an inert gas atmosphere, thus decomposing the polymer matrix. A small portion of the carbon fibers was transferred onto a microscope glass slide and images of fibers were taken using a Leica DMI 5000 M optical microscope (Leica Microsystems GmbH, Wetzlar, Germany). Low magnification micrographs (100×) were then analysed using Image J® software. Approximately 150 fibers were measured in order to obtain reliable results.

The microstructure of the filaments and 3D printed samples was investigated by optical microscopy. Cross sections of pristine filament and dog-bones (one for each printing architecture) were obtained by cutting them with Buehler IsoMet® 4000 precision saw (Buehler, Lake Bluff, IL, USA). The samples were then mounted in epoxy resin and polished using standard metallographic preparation techniques. Optical images were taken at different magnification to observe the layered structure, the porosity and the fiber orientation. Void fraction analyses were performed with Image J® software. X-Ray Diffraction (XRD) measurements were performed on the 3D printed specimens, using a PANalytical PW3040/60 X'Pert PRO diffractometer (Cu-K_α radiation at 40 KV and 40 mA, 2θ range from 10° to 70° with a step size of 0.013°).

The tensile properties of the FDM samples were determined by testing four dog-bone samples for each studied printing architecture using a universal testing machine (MTS Criterion Model 43, MTS Systems S.r.l., Italy) equipped with a 5 kN load cell. Tensile tests were carried out according to ISO 527-4 standard with a strain rate of 1 mm/s; a 25 mm gage-length extensometer was used for strain measurements.

The morphology of the fracture surfaces of tensile specimens and cryo-fractured filament was investigated by using a field emission electron scanning microscope FESEM Zeiss MERLIN (Carl Zeiss Microscopy GmbH, Jena, Germany) at an acceleration voltage of 15 kV. FESEM analyses were also performed to examine the morphology of the conductive tracks after laser writing, and to compare the characteristics of carbon fibers networks between tracks produced on samples with different architectures. In order to avoid charging, all samples were coated with platinum. The topography of the tracks was studied by means of a Leica DCM8 confocal profilometer (Leica Microsystems Gmbh, Germany); MountainsMap software was used to perform the image analysis.

Electrical resistance measurements were carried out using a two-point probe digital multimeter Keithley 2700 (Keithley Instruments Inc., Cleveland, OH, USA) with a full scale of 120 MΩ. A small amount of silver paint was deposited at the beginning and the end of each track to improve contacts. The resistance values were normalized on track length, thus obtaining the surface electrical resistance per unit length (R). Similar tests were also performed on 3D printed samples to determine their electrical behaviour before laser functionalization.

3. Results and discussion

3.1. Filament characterization

The thermal, physical and microstructural properties of the feedstock filament were investigated to assess the validity of the process parameters adopted during the 3D printing process. Moreover, the characterization of the fibers (in term of quantity, length and orientation within the filament) is useful to understand the microstructure and mechanical properties of FDM build part.

The DSC curve of Carbon PA filament is shown in Fig. 2A, while thermal transition temperatures and crystalline fraction are listed in Table 2. The melting peak can be clearly observed in the heating curve, while an exothermal peak which corresponds to polymer crystallization was detected during sample cooling. The first part of the DSC heating curve is highlighted in the inset of Fig. 2A. The glass transition temperature (T_g), measured as the inflection point of the curve, was 52 °C. The thermal transition temperatures obtained from DSC analysis (Table 2) clearly indicated that the matrix used in the composite is a polyamide 6 [31,32].

Table 2
Thermal properties of the composite measured with DSC and TGA techniques.

DSC (heating)			DSC (cooling)		TGA (matrix pyrolysis)	
T_g (°C)	T_m (°C)	ΔH_m (J/g)	X_C (%)	T_C (°C)	T_{onset} (°C)	T_{max}(°C)
52.3	232.9	43.4	22.6	183.1	352.6	410.5

The thermal stability and fiber content of the filament were investigated by thermal gravimetric analysis using the procedure described in Section 2.2. The weight loss and first derivative curves are depicted in Fig. 2B. Three main degradation steps are clearly visible: the first one occurs above 350 °C (first step of heating under argon flow) and can be attributed to the main-chain degradation of polyamide matrix in inert atmosphere; the onset temperature for polyamide degradation (T_{onset}) and the temperature of maximum weight loss rate (T_{max}) respectively are reported in Table 2.

The second step occurs at around 400 °C in air atmosphere and it is associated to the oxidation of the residual carbonaceous species left after matrix pyrolysis [33,34]. The last one is due to carbon fiber oxidation that usually takes place in air between 500 °C and 900 °C, depending on their graphitic structures [35]. These results show that the fiber content in the filament is about 15 wt.%, while 4 wt.% of another inorganic filler is also present. The results of the thermal analysis demonstrate the validity of the process parameters used during FDM printing. The relatively high extrusion temperature (300 °C) is justified by the high melting temperature of polyamide 6 and the presence of carbon fibers; however, the value is lower than the onset of thermal degradation of the filament (Table 2). The bed temperature (45°) was set just below the glass transition to avoid thermal distortion at the end of the print.

X-Ray diffraction of the filament showed the presence of an intense peak belonging to γ- crystalline form at 2Θ = 21.5° and two less intense peaks characteristic of the α-crystal form at 2Θ of approximately 20° (200) and 23.7° (202/002) respectively [36]. Additional peaks at 2Θ equals to 18.3°, 30.1°, 35.5°, 43.1°, 57.0° and 62.6° were observed in the XRD pattern; they can be attributed to magnetite (ICDD card number 01-088-0866). SEM-EDS analyses performed on the starting filament and on the residue coming from heating samples at 800 °C in inert atmosphere (Section 2.2) evidenced the presence of particles with size close to 1 μm. The semi-quantitative EDS analyses displayed that these particles were rich in iron and oxygen (Fe = 31 wt.% and O = 24 wt.%). These outcomes confirmed that magnetite was used as a filler for the processing of Carbon PA filament. The presence of this compound is not common in polymeric materials; however, it can be added as multi-functional filler to process high-density components to be used for aesthetic purposes, sound and vibration damping. This filler

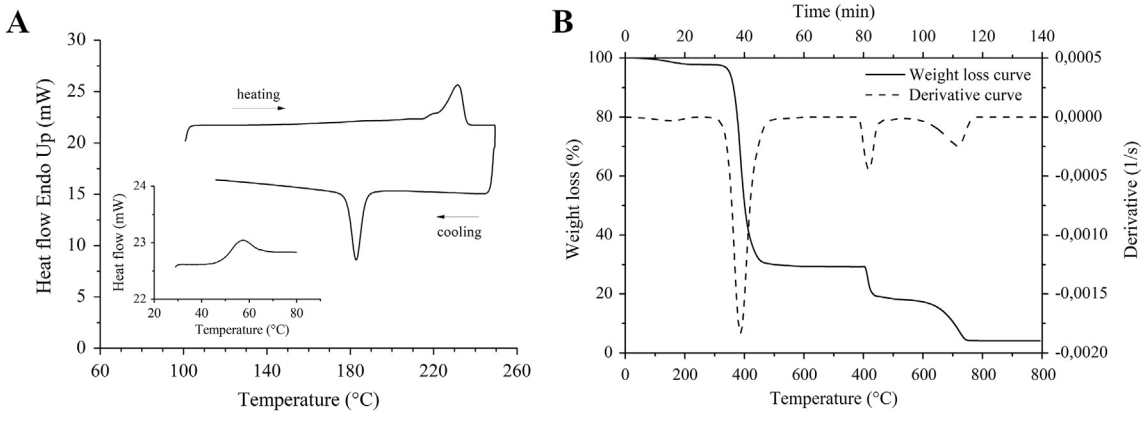

Fig. 2. Characterization of Carbon PA filament: (A) heating/cooling DSC curves and (B) TGA (straight line) and Derivate-TGA (dashed line) curves.

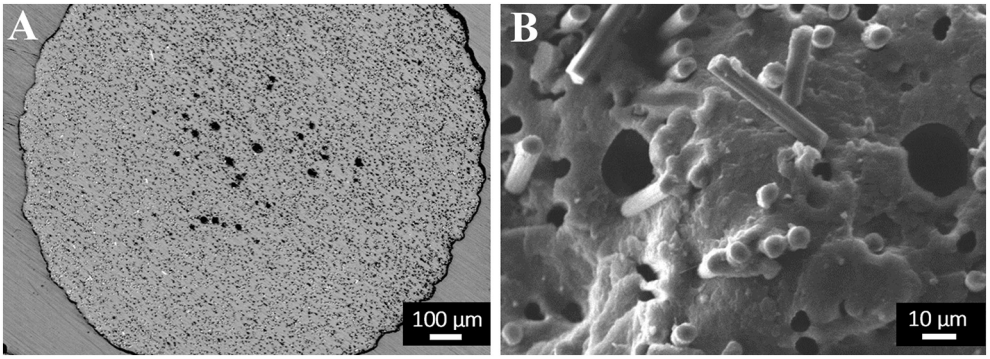

Fig. 3. (A) Optical micrograph of the polished filament cross-section and (B) FESEM micrograph of the cryogenically fractured filament, showing pores and carbon fibers aligned in the extrusion direction.

is also used with the aim of improving thermal, electrical and radiation blocking properties [37].

Optical and FESEM micrographs showing the cross section of FDM filament, are reported in Fig. 3. From the optical micrograph (Fig. 3A), it is possible to see the round-shaped filament (nominal diameter of 1.75 mm) and some pores located in the middle of the cross section. The presence of these voids (the image analysis revealed a porosity of 4.8 ± 0.2%) is probably related to gas evolution during the extrusion process [4].

The fracture surface of the filaments (Fig. 3B) shows the pull out of the carbon fibers, and their fairly good alignment to the filament length. This preferred orientation is likely further strengthened during the printing process of the components, because of the shear stress occurring during filament extrusion and deposition enhances the fiber orientation. This phenomenon is referred as flow-induced orientation [5]. Small circular cavities, caused by fiber pull out, are clearly visible on the fracture surface. The brakeage of pulled out fibers is responsible for the presence of fiber fragments lying on the fracture surface. Larger voids attributable to matrix porosity can also be seen.

Fig. 4A shows an optical micrograph of the carbon fibers after polymer pyrolysis, that allows to evaluate their diameter (about 6.5 μm). The fibers present a slightly asymmetric length distribution (Fig. 4B) with an average length of 94 μm. It is worth noting that these fibers are similar or slightly longer than the ones successfully used to enhance the tensile modulus and strength of ABS, PLA and PETG 3D printed parts (50–100 μm) [4,11].

3.2. 3D printed parts characterization

The mechanical properties and the porosity of 3D printed specimens produced with [±45], [0] and [45, 0, −45, 90] architectures are compared in Table 3. Significant differences in tensile modulus and strength were observed; the highest values, 11.7 GPa and 105.8 MPa respectively, are reported by setting a raster angle of 0°. Different printing architectures, such as [±45] and [45, 0, −45, 90] ones, should be adopted to improve the mechanical isotropy of the components; however, in both cases stiffness and strength are lower.

In order to compare the mechanical properties of Carbon PA samples with existing literature, tensile strength and Young's modulus values for several discontinuous CFRPs printed through FDM are summarized in Table 4. These data show that Carbon PA parts have superior mechanical properties compared to other discontinuous CFRPs; this confirms the potential applications of this material for the manufacturing of load-bearing components through FDM.

The differences in stiffness and tensile strength between [0], [±45], [0, 45, 90, −45] printed specimens (Table 3) can be easily explained by analysing the orientation of the fibers within the parts with respect to the loading direction (i.e. sample axis). The optical micrograph of the polished cross-section of [+45, 0, −45, 90] sample (Fig. 5A) clearly shows the effect of different fiber orientation on the microstructure. In fact, the layered structure of the sample and the cross section of the fibers can be clearly observed. The latter changes from a rectangular shape in layers printed at 90° raster angle to elliptical and circular ones, observed in layers with filaments placed at ±45° and 0° respectively. It has been reported that the analysis of the elliptical footprints left by fibers on a polished surface gives qualitative and quantitative indications on their orientation in composite [10,39]. Therefore, it can be concluded that the FDM process promote the alignment of fibers along the printing direction, that varies from one layer to another in a regular fashion in the [45, 0, −45, 90] architecture (Fig. 5A).

This peculiar microstructure was already observed in CF/ABS and CF/PLA composites processed through FDM [10,13–16]. In fact, during the

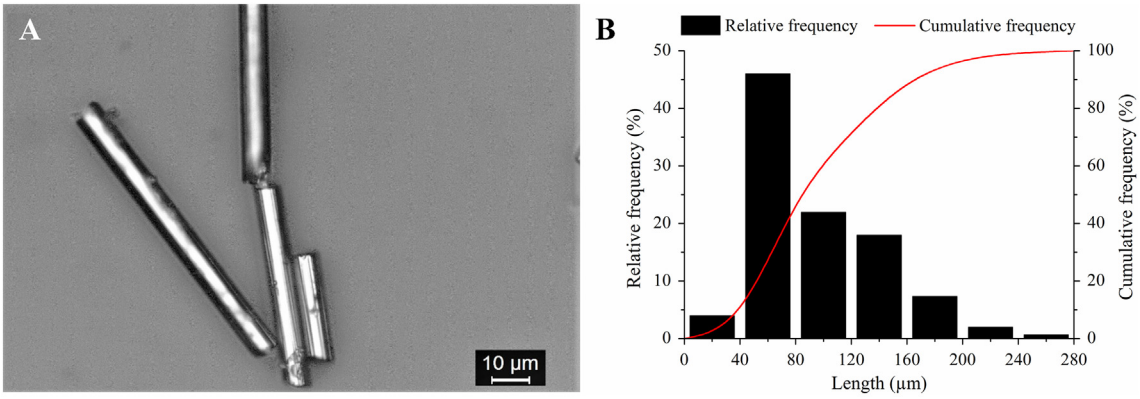

Fig. 4. (A) Optical microscope images of carbon fibers after matrix removal through pyrolysis and (B) fiber length distribution obtained with Image J® software.

Table 3
Tensile properties and porosity of 3D printed specimens with different architectures.

Printing architecture	Elastic modulus (GPa)	Tensile strength (MPa)	Strain at break (%)	Porosity (%)
[±45]	7.73 ± 0.06	72.9 ± 12.2	1.37 ± 0.37	13.8 ± 0.9
[0]	11.71 ± 0.55	105.8 ± 4.0	1.16 ± 0.07	11.3 ± 0.5
[+45, 0, −45, 90]	7.98 ± 0.07	67.6 ± 1.3	0.92 ± 0.05	10 ± 1.1

Table 4
Summary of the highest tensile strength and modulus values reported to date for discontinued CFRPs printed with [0] and [±45] architecture.

Material	Filler loading (%)	Printing architecture	Elastic modulus (GPa)	Tensile strength (MPa)	Ref.
CF/PA12	10	[0]	3.6	93.8	[12]
CF/PA6	20	[0]	6.2	52.0	[38]
CF/ABS	40	[0]	13.7	67.0	[10]
CF/PLA	13	[0]/[±45]	9.3/5.2	68.4/54.6	[11]
CF/PETG	18	[0]/[±45]	8.5/4.2	68.3/50.9	[11]

printing process the thermoplastic matrix melts down inside the extruder. As a result, of the shear stress and velocity gradients within the melt, the fibers tend to align along the extrusion direction. Numerical simulations [40] also demonstrate that fibers maintain a good alignment outside the nozzle, in spite of die swelling phenomenon that only slightly affects their orientation. The FESEM examination of the fracture surface of a [±45] sample further highlights the preferred orientation of the fibers (Fig. 5B and C). In addition, the high magnification micrograph (Fig. 5C) shows that the pulled out fibers are frequently covered with a thin polymeric layer. This indicates that a mechanical interlocking was established between fibers and matrix, and an effective stress transfer can be expected.

The reported results reveal that processing fiber reinforced polymers through FDM allows to tailor the mechanical properties of the composite by changing the direction of extruded paths in the part. It is thus possible to control fibers orientation, differently from traditional manufacturing techniques such as injection or compression moulding. It can be concluded that the FDM-printed material has similar mechanical behaviour compared to unidirectional fiber reinforced laminates. In fact, samples printed at 0° benefit from a greater reinforcement effect as carbon fibers are preferentially aligned in the tensile loading direction. This strengthening effect decreases as a function of the angle between the extruded beads and the applied load.

Fig. 5A also reveals the presence of a significant number of pores. Voids represent common defects in FDM build parts and their morphology and formation mechanisms are deeply discussed in the literature for unreinforced and reinforced polymers [4,10,14]. Various authors recognized several types of voids in 3D printed composite parts:

- Inter-beads voids: physical gap at layer/layer interfaces or triangular gap among filaments, generated by die-swelling and incomplete sintering of adjacent beads.
- Inner-beads voids: smaller pores inside the extruded filaments caused by gas escaping [4] or partially independent movement of fibers and matrix during printing [10].
- Cylindrical voids attributed to fibers pull-out.

These kinds of voids can be easily observed in the FESEM micrographs of samples with [±45] architecture (Fig. 5B and C). Inter-beads voids which consist in large pores among layers are indicated as pore of type 1 (Fig. 5B); on the contrary, triangular gap among adjacent beads are not present because the addition of fibers decreases the die swell and increases the thermal conductivity of the material. This helps the surrounding beads to soften and improve their coalescence [10]. In addition, smaller inner-beads voids showing the same morphology of the pores found in the feedstock filament (Fig. 3B) were observed (pore type 2 in Fig. 5B). The size and shape of these voids suggest that their formation mechanism is related to gas escaping during the extrusion experienced both in filament production and FDM processing.

The polished cross-sections of the 3D printed dog-bones showed porosity volume fractions varying in the range from 10% to 14% (Table 3), depending on the building architecture. These variations can be attributed to differences in inner-beads void distributions (i.e. size and shape) [16,41], but their effect on the mechanical behaviour should be negligible with respect to fiber orientation.

The electrical properties of the 3D printed plates were moreover assessed. The specimens, independently from their printing

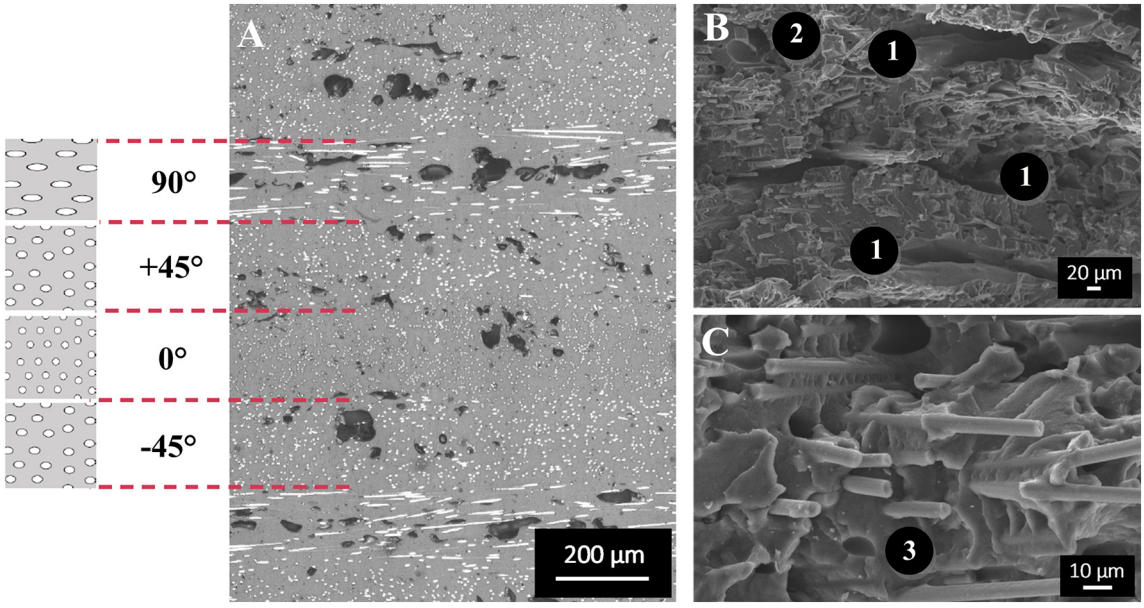

Fig. 5. (A) Optical micrograph of the polished surface of dog-bone cross-section printed with [+45, 0, −45, 90] architecture and (B,C) FESEM micrographs of the fracture surface of tensile samples printed at [±45°]. In fig. (A) the cross sections of the fibers observed within the layers are schematically sketched. In (B) different type of voids are highlighted: (1) inter-bead voids, (2) inner-beads voids and (3) cavity caused by fiber pull-out.

Table 5
Influence of printing architecture and laser writing direction on surface electrical resistance of tracks processed with the same laser parameters (P = 10%, v = 100 mm/s, N = 10). Average track resistance is reported as median value of all writing directions.

Printing architecture	R (kΩ/cm) LW direction 0°	R (kΩ/cm) LW direction 90°	R (kΩ/cm) LW direction 45°	R (kΩ/cm) LW direction −45°	$R_{average}$ (kΩ/cm)
[±45]	1.37 ± 0.09	3.52 ± 2.00	1.87 ± 0.16	1.32 ± 0.24	2.02 ± 0.08
[0]	3.33 ± 1.95	46.51 ± 21.71	12.94 ± 3.30	17.64 ± 3.22	20.11 ± 3.26
[+45, 0, −45, 90]	2.50 ± 0.58	6.12 ± 1.18	3.54 ± 1.56	3.65 ± 0.23	3.95 ± 1.65

architecture, showed very high surface electrical resistance (>120 MΩ/cm). Therefore, the insulating behaviour of Carbon PA parts allows the exploitation of laser writing to obtain conductive tracks preventing any risk of short circuit.

3.3. Laser writing of conductive tracks

3.3.1. Effect of sample architecture on track resistance

Table 5 reports the surface electrical resistance of conductive tracks produced on 3D printed plates fabricated with different printing architecture. Tracks were produced by using the same laser parameters and varying the writing direction with respect to x-axis. The definition of writing direction of a printed track is schematically depicted in Fig. 6D. Four writing directions were considered in order to assess the variability of resistance values as a function of track orientation. The laser parameters (P = 10%, v = 100 mm/s, N = 10) adopted were previously used for obtaining conductive tracks on CNTs reinforced polymer composites [27,42].

The results can be easily explained studying the morphology of the tracks obtained at 0° writing direction (Fig. 6A, B and C). As described in the previous sections, the samples were processed by FDM varying the printing architecture. This leads to different orientations of beads and fibers within the stacked layers. When [0] architecture is adopted, the fibers are aligned in the same direction. On the contrary, their orientation changes layer by layer when [±45] or [+45, 0, −45, 90] architectures are used. FESEM micrographs indicate that the ablative action of the laser involved at least two layers of the material (Fig. 6A and B). As a consequence of laser irradiation, carbon fibers form percolative networks with different morphology depending on the specific layered architecture of the 3D-printed plates (Fig. 6). These morphological differences entail a dissimilar arrangement and entanglement of fibers, and should result in greater or lesser probability of electrical conduction.

Samples printed according to ±45° raster angle exhibit a denser and more interconnected network of fibers (Fig. 6B) and thus they show the lowest surface electrical resistance. Moreover, the electrical behaviour of this sample is only limited influenced by LW direction (Table 5). The tracks produced on plates with the more complex [+45, 0, −45, 90] architecture exhibit a similar interconnected network of fibers (Fig. 6B), but the electrical resistances are slightly higher (Table 5). The sample printed at 0° raster angle (Fig. 6C) displays no visible network in the middle of the track, although fibers are present on the walls of the tracks. This unexpected morphology is probably a result of the [0] printing architecture. In fact, it seems that the fibers in the middle of the track can be easily removed after laser writing because they are no more embedded in the polymer matrix. Despite the absence of an interconnected network, the fibers placed on the track walls can provide some electrical conductivity. However, resistance values are one order of magnitude higher compared with the other architectures (Table 5).

Therefore, the samples printed with ±45° raster angles provided the best performances in terms of track conductivity and reproducibility along different writing direction. For this reason, this printing architecture was selected to optimize the laser writing process.

3.3.2. Optimization of laser writing process

The first objective of the process parameters optimization was to obtain conductive tracks with surface electrical resistance lower than 1 kΩ/cm. In fact, this is the threshold value for the transmission of low-power electrical signals.

A systematic study was carried out to investigate the influence of laser parameters on the electrical resistance of the tracks. Laser defocusing and frequency were set at a constant value of 0 mm and 20 Hz respectively. The curves depicted in Fig. 7 display the effect of laser power (Fig. 7A), writing speed (Fig. 7B) and number of repetitions (Fig. 7C) on the resistance of tracks produced on plates printed with [± 45] architecture.

The graphs show a progressive reduction of track electrical resistance with increasing laser power and number of repetition or decreasing the writing speed. These findings confirm the results of previous studies on CNTs/polymer composites [26–28,42]. The conductive tracks reached low electrical resistance values (~0.02 kΩ/cm) for samples treated by using 15% of maximum laser power and 150–100 mm/s

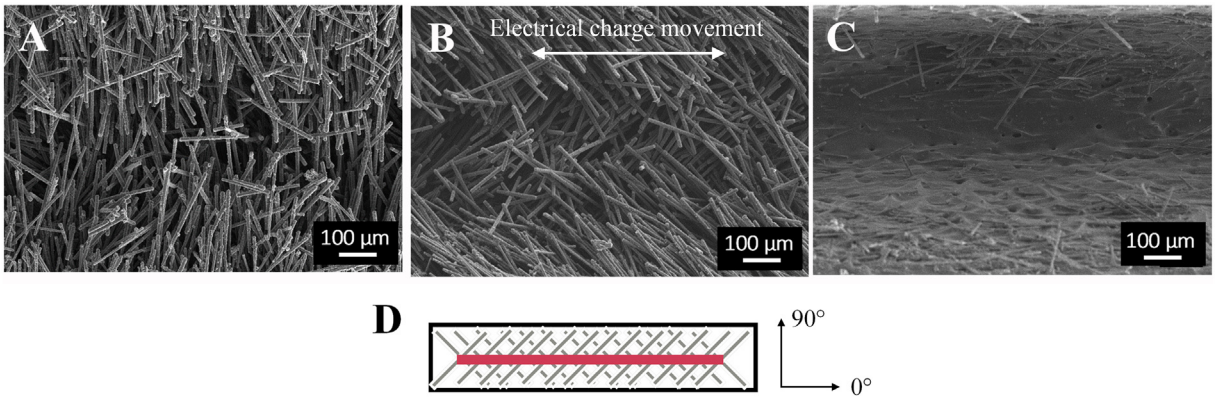

Fig. 6. FESEM micrograph showing fiber arrangement inside the tracks produced on plates with different printing architectures: (A) [+45, 0, −45, 90], (B) [±45] and (C) [0]. (D) Definition of writing direction of a printed track. A sample with [±45°] printing architecture (grey pattern) and a single track at 0° writing direction (red line) is schematically sketched. (For interpretation of the references to colour in this figure legend, the reader is referred to the web version of this article.)

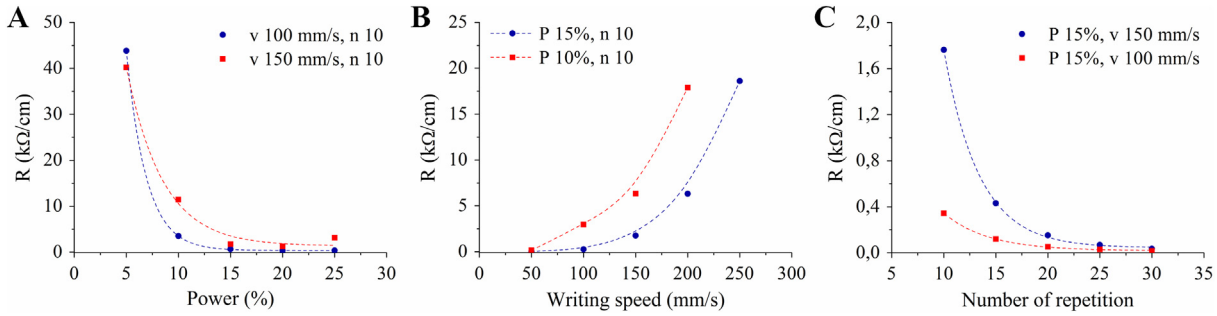

Fig. 7. Electrical resistance of conductive tracks obtained on carbon fiber/polyamide plates as a function of: (A) laser power, (B) writing speed and (C) number of repetitions.

writing speed for 25–30 times. Lower values of resistance (<10 Ω/cm) were found using more severe laser treatments, but the samples revealed unacceptable aesthetic quality. Negligible values of inter-track conductivity were recorded (R > 120 MΩ).

Good aesthetic quality, defined as absence of morphological defects and distortion of the sample after laser processing, is an essential requirement to qualify the parts for industrial applications. The conductive tracks are usually written on the internal surface of the component and therefore they are not visible; in fact, only the not treated side is directly exposed. However, the use of not optimized laser parameters can result in a too deep tracks which can damage the exposed surface.

Therefore, new trials were performed setting a fixed power of 15%. Several writing speeds (from 50 mm/s to 250 mm/s) were tested and the track resistance was measured at increasing number of repetitions. For each combination of power and writing speed the trial was interrupted when the track did not show acceptable aesthetic quality. Two main aspects need to be considered to evaluate the quality of the surface which is opposite with respect to the laser treated one: morphological modifications such as alteration of colour or of surface finish, and the occurring of deformation of component due to the laser action. A visual inspection of the surfaces after the writing of tracks was performed; samples were classified into one of the following aesthetic categories:

- Excellent": no morphological defects and no distortion were observed.
- "Good": minor morphological defects were reported, but the part kept its planarity.
- "Acceptable": minor morphological defects accompanied with a slight deviation from planarity were observed. However, the distortion of the part can be prevented by fixing the sample through a clamping system during the laser treatment.
- "Not acceptable": significant variation of morphological properties and deformation were observed.

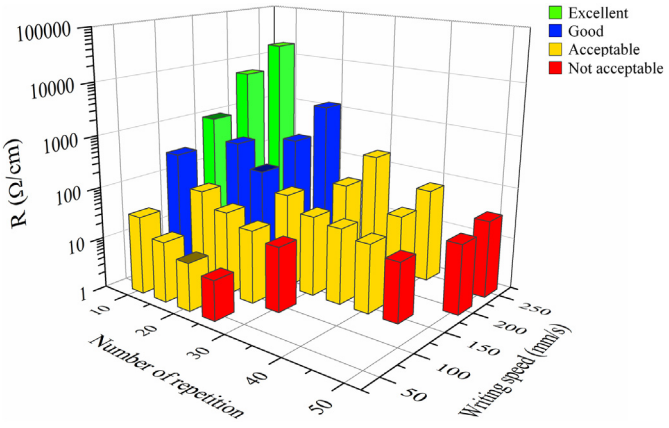

Fig. 8. Electrical resistance of conductive tracks as a function of writing speed, number of repetition and aesthetic quality. Columns with a darker top highlight the best treatments for "Excellent" (blue), "Good" (green) and "Acceptable" (yellow) aesthetic categories. (For interpretation of the references to colour in this figure legend, the reader is referred to the web version of this article.)

The results, depicted in Fig. 8, highlight the influence of number of repetitions and writing speed on electrical resistance and aesthetic quality of the tracks.

On the base of these outcomes, it is possible to establish the processing conditions which grant the lowest resistance within each aesthetic category. These sets of laser parameters, labelled as T1, T2 and T3, are reported in Table 6.

Because of T1 treatment did not allow to reach electrical resistance lower than 1 KΩ/cm, the other sets of laser parameters (T2 and T3) were identified as the best processing conditions for obtaining conductive tracks on Carbon PA plates. These tracks exhibited extremely low resistance per unit length, equal to 0.15 KΩ/cm and 0.008 KΩ/cm for T2 and T3 laser treatment respectively. These values are among the lowest ever obtained by laser writing on metal-free polymeric composites. Particularly, they are comparable or even better than those reported for polymers reinforced with nanofillers with very high intrinsic conductivity (from 7.0 to 0.9 KΩ/cm) [28]. However, also the nature of polymeric matrix seems to exert some influence on the track conductivity, as a resistance of 0.02 kΩ/cm was obtained by laser treatment on injection-moulded PC/ABS blends reinforced with CNT [27].

3.3.3. Characterization of laser printed tracks: topography and reproducibility

Because of tracks produced by using T2 and T3 set parameters showed higher conductivity with respect to the target value and aesthetic features suitable for the realization "in situ" of electrical circuits by laser scribing, their characteristics were more deeply investigated in terms of morphology and resistance reproducibility. Fig. 9A shows the fractures cross section of the track produced by using T2 parameters set. The FESEM micrograph shows that the track depth is about 300 μm, therefore laser ablation involved the first two layers of the material; moreover, a regular track profile with an interconnected network of carbon fibers placed on the track walls can be observed.

Topographic images of the conductive tracks allow to measure their width and depth. The sample treated by using a writing speed of

Table 6
Sets of laser writing parameters granting the best electrical performances of conductive tracks with "excellent", "good" and "acceptable" aesthetic quality.

Laser treatment	Power (%)	Writing speed (mm/s)	Number of repetitions	Resistance (kΩ/cm)	Aesthetic quality
T1	15	150	10	1.08 ± 0.25	Excellent
T2	15	150	20	0.15 ± 0.03	Good
T3	15	50	20	0.008 ± 0.001	Acceptable

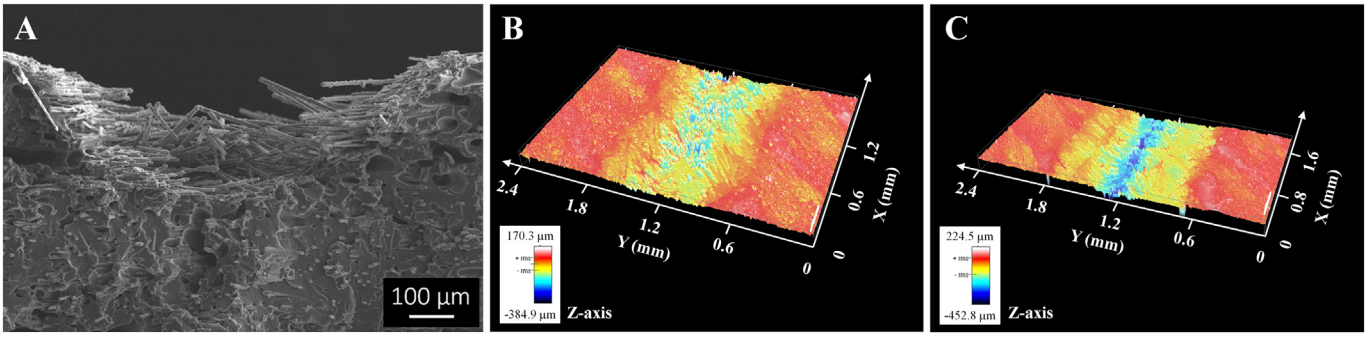

Fig. 9. (A) FESEM micrographs showing the cross section of the track obtained with T2 set of parameters and (B,C) surface topography (3D micrographs) of two conductive tracks printed with different laser parameters: (B) T2 and (C) T3. The colour map shows the depth of the track along the z-axis.

150 mm/s, 20 repetitions and 15% of maximum laser power shows a track with a mean depth of 228 µm and a width of 1 mm (Fig. 9B), The sample treated at the lowest writing speed (50 mm/s) reveals a wider track (1.7 mm) with an average depth of 334 µm (Fig. 9C), as a result of the higher laser energy input. Experimental and theoretical results reported by Ruan et al. [43] confirmed that laser power and irradiation time strongly affect the size and morphology of features created by direct laser writing on polyimide.

In order to qualify laser writing for industrial applications the reliability of the process entails great importance. The variation of electrical resistance between tracks written on different plates is depicted in Fig. 10A. Maximum variations of 0.147 kΩ/cm and 0.010 kΩ/cm were observed for samples processed according to T2 or T3 treatments respectively. Anyway, the resistance values were always significantly lower than 1 kΩ/cm. These differences probably arise from an inhomogeneous voids distribution, resulting from the local and time-dependent variations of temperature occurring during the printing process. This effect is particularly evident when large batches are printed in a single build [44].

The influence of track length on the resulting electrical resistance is reported in Fig. 10B; a moderate increase of the electrical resistance with the increase of the track length was observed. The resistance increase as a function of the track length was 0.010 kΩ/cm and 0.075 kΩ/cm for T2 or T3 sets of samples respectively; this increment is due to the presence of defects: longer is the track, higher is the possibility to detect porosity or a local decreasing of fiber concentration which lower the resistance values. However, in all the cases the resistance was much lower than the threshold value of 1 kΩ/cm.

Inter-track resistance was always four order of magnitude higher than the track resistance (values higher than 120 MΩ, namely outside of the measurement range were collected); therefore, any risk of short circuits can be excluded.

3.4. Comparison of laser tracks obtained on samples fabricated by fused deposition modelling and injection moulding

In order to compare the effect of laser functionalization on components processed by innovative additive manufacturing and more traditional processing routes, Carbon PA plates were processed by injection moulding. These latter were obtained by using starting filament and scraps; this allow the total reuse of production wastes. Despite the FDM process involves the melting of the filament, the extrusion temperature was lower than the onset degradation temperature of Carbon PA (Table 2). Therefore, the experienced thermal cycle did not significantly affect the properties of the material. On the base of previously obtained results (Section 3.3.1) the track resistance is mainly affected by the morphology of fibers network after laser irradiation.

The results of laser writing of conductive tracks on samples produced by FDM and injection moulding (IM) are summarized in Table 7. The treatments were performed using T2 and T3 sets of parameters as they provided the best compromise between electrical functionality and aesthetic quality. The electrical performances of conductive tracks realized on injection moulded plates are similar or even worse than those achieved on the 3D-printed samples. It was previously observed that the fiber orientation influences the electrical conductivity of FDM samples. Therefore, the obtained results can be explained by considering the different arrangement of fibers within the tracks produced on FDM and IM samples respectively. In components produced by injection moulding the fibers are generally aligned

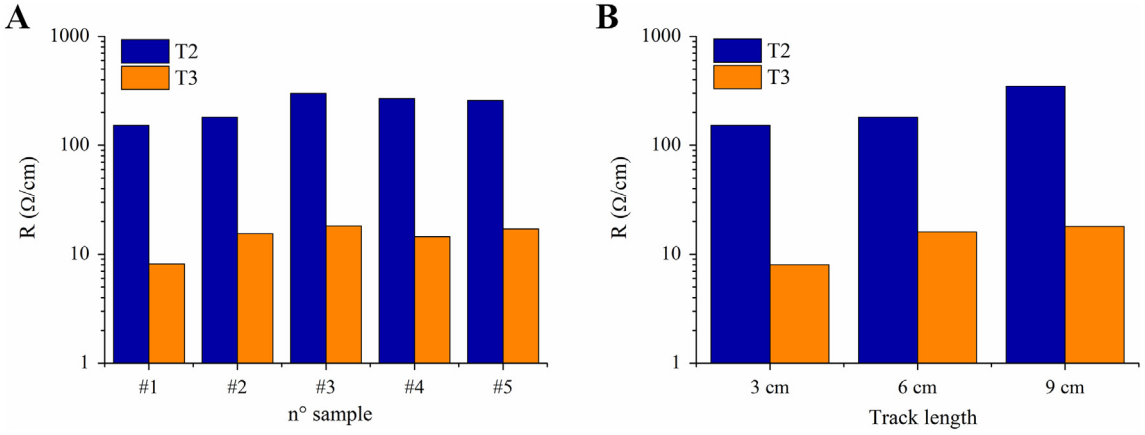

Fig. 10. Electrical resistance (logarithmic scale) of tracks treated according to T2 and T3 laser parameters: (A) reproducibility between different plates and (B) resistance of track with different length (3, 6 and 12 cm).

Table 7
Surface electrical resistance of tracks obtained on both FDM and injection moulded plates using T2 and T3 set of laser parameters.

Laser treatment	Power (%)	Writing speed (mm/s)	Number of repetitions	R_{FDM} (kΩ/cm)	$R_{injection\ moulding}$ (kΩ/cm)
T2	15	150	20	0.152 ± 0.026	0.245 ± 0.031
T3	15	50	20	0.008 ± 0.001	0.008 ± 0.001

to the flow direction [39], while in FDM parts their orientation changes as a result of the adopted printing strategy. This leads to the formation of interconnected networks of fibers within the track (Fig. 6A and B). Although IM process involves the preferential orientation of filler in the extrusion direction, this effect is less significant in IM samples with respect to FDM ones. This results in resistance values for IM specimens which are comparable or lower with respect to those observed for FDM ones. Therefore, it can be safely concluded that FDM does not compromise the effectiveness of laser functionalization.

3.5. Comparison between laser writing and competing techniques

A direct comparison of the electrical properties between laser writing and existing method for processing multifunctional composites with embedded conductive tracks is reported in Table 8.

Most of the literature is focused on the electrical behaviour of conductive tracks in terms of resistivity, although data regarding resistance per unit length are also reported. The resistivity of laser written tracks was determined using the Eq. (2):

$$\rho = R \cdot A \tag{2}$$

where R is the resistance per unit length and A is the effective area of carbon fibers network inside the track, which was measured by image analysis (Fig. 9A). The obtained values (~10^{-4} Ω·m) are in good agreement with the resistivity of chopped carbon fibers (~10^{-5} Ω·m) [52].

Table 8 shows that laser written tracks have inferior electrical performances than copper wirings, metal paste or conductive inks used to produce printed circuit on polymeric substrate. However, the resistance per unit length achieved after laser writing is comparable to that of conductive filaments specifically developed for 3D printing of electronic sensors. These values allow the transmission of low power signal in simple electric devices, such as sensors, buttons or antennae [23,24]. Moreover, laser writing reveals important advantages over these competing techniques:

- Process complexity and environmental impact are reduced. In fact, copper wirings and conductive inks are not required to produce electrical circuit. The parts can be easily recycled since the same thermoplastic polymer composite act both as insulating substrate and active electronic components.
- Unlike ink jet printing and direct writing, post-treatment of the tracks (i.e. sintering of conductive inks at temperature up to 200 °C), are not required to obtain the desired conductivity [47–49]. Therefore, engineering and commodity polymers, such as ABS, nylon or polypropylene, can be safely used as dielectric substrate without constraint on their thermal properties (i.e. high heat deflection and glass transition temperature) that would greatly limit the material choice.
- Laser writing is particularly effective for fabricating embedded electronics components in FDM substrate. The inherent porosity and roughness of FDM parts prevent the direct use of conductive inks on untreated surfaces. In fact, the inks will spread into surface beads and across stacked layers throughout the void, thus causing electrical short circuits [46]. Alternatively, it is possible to leave hollow channels or use sacrificial materials in desired area during FDM printing. However, post-printing integration processes, such as metal wires embedding or liquid metal paste filling, are needed to obtain the conductive pattern [46,50].
- Laser writing was also exploited to improve the piezoresistive response of polymer nanocomposites. Distinct conductive tracks and piezoresistive areas could be created, thus developing a "touch sensitive integrating switch" material [24,28,42].

Table 8
Summary of reported resistivity data for conductive tracks embedded in polymeric substrate produced using different technologies.

Technology	Material	R (Ω/cm)	ρ (Ω·m)	Ref.
Laser writing	None	8	$3.2 \cdot 10^{-4}$	Table 6
FDM	Conductive filament	9	$2.2 \cdot 10^{-2}$	[45]
Wire embedding	Copper wire	5×10^{-3}	$1.7 \cdot 10^{-8}$	[46]
Ink jet printing	Silver ink	–	$9 \cdot 10^{-8}$	[47]
Ink jet printing	Silver ink	–	$3 \cdot 10^{-7}$	[48]
Direct writing	Silver filler epoxy adhesive	–	$4 \cdot 10^{-6}$	[49]
Liquid metal paste filling	Silver suspensions	0.18	$3.5 \cdot 10^{-6}$	[50]
Hybrid AM system	Silver paste	0.05–0.22	$1–3 \cdot 10^{-6}$	[51]

It is also worth noting that 3D printing of continuous carbon fiber reinforced composites by using FDM systems is promising for the development of multifunctional parts, due to the higher strength and conductivity of continuous fibers. However, these systems do not provide suitable resolution for obtaining conductive paths within the part and allow the deposition of the fibers only along selected patterns, such as concentric or unidirectional ones [21]. On the contrary, laser writing creates tracks according to paths that can be modified as desired; therefore, it represents a more accurate and versatile method for the production of electrical circuits with complex geometries [26]. An alternative approach was developed to embed continuous carbon fiber tows into PLA parts during the FDM process [53]. In these components, carbon fibers serve as structural reinforcement and sensory agents thanks to their piezoresistive behaviour. However, the extensive pause required to manually place the fiber tows during the printing process may cause weaker interlayer bonding, thus inducing structural weak points.

4. Conclusions

An innovative manufacturing process, based on fused deposition modelling and laser writing technologies, was successfully developed to produce metal-free conductive tracks embedded on the surface of carbon fiber/polyamide composite parts.

The microstructural analyses of 3D printed samples revealed that FDM induces the alignment of carbon fiber along the printing direction; inter-beads and inner-beads voids were also observed. The preferred orientation of carbon fibers, is responsible for the variation of mechanical properties among samples processes with different printing architectures. In fact, samples printed using a 0° raster angle show the highest tensile strength and elastic modulus because the fibers are aligned along to the loading direction. The reinforcing effect of the fibers decreases in other printing architectures.

The effect of laser writing process on 3D printed carbon fiber/polyamide composites was widely investigated though the measurements of tracks electrical resistance and the evaluation of samples morphology. The characteristics of percolation networks that carbon fibers form inside the tracks ARE affected by the printing architecture of FDM samples. The highest conductivity was obtained when filaments are deposited with alternating angles of ±45°, leading to an interconnected networks of carbon fibers. This printing strategy, and the resulting [±45] architecture also guaranteed small variations of track conductivity as a function of laser writing direction.

Moreover, the resistance of the tracks greatly depends on the adopted process parameters. The electrical conductivity increases as a

function of laser pulses energy increase. However, excessive energy inputs give rise to unacceptable aesthetic quality (alteration of surface finish or colour and deformation of exposed surface can be observed); therefore, a compromise between parts integrity and functionality needs to be achieved. Processing parameters which results in good aesthetic quality combined with very low electrical resistance (from 0.152 KΩ/cm to 0.008 KΩ/cm) and no conduction between adjacent tracks, were established. To date, these values are among the lowest ever obtained by laser writing on metal-free polymer composites; moreover, they are comparable to those achieved using nanofillers with very high intrinsic conductivity.

The electrical performance of the tracks obtained on injection moulded plates is slightly lower compared with laser treated FDM samples. Therefore, it can be concluded that the inherent microstructure of FDM built parts in terms of fiber orientation and porosity do not compromise the effectiveness of the laser functionalization.

The main advantages and drawbacks of the proposed method were assessed by comparing the results obtained with existing literature. For this purpose, the mechanical properties of polymer composites processed through FDM and the electrical performances of conductive tracks embedded in dielectric substrate by using different technologies were reviewed.

The achieved conductivity values demonstrate the possibility of integrating conductive tracks obtained via laser writing into high-strength polymer composite parts produced by FDM. The tracks, created according to desired computer-controlled paths, can be used to produce simple electric devices (such as buttons, sensors, antennae, etc.). The latter can be directly embedded in polymeric components used in automotive, aeroplanes and in domestic appliances. Moreover, the conductive tracks are easily integrated into the substrate without the use of copper connections, thus offering significant weight reductions and simplifying both the production process and the end-of-life disposal of the component.

CRediT authorship contribution statement

Federico Lupone: Investigation, Writing - original draft. **Elisa Padovano:** Writing - review & editing, Visualization. **Antonino Veca:** Conceptualization, Supervision. **Lorena Franceschetti:** Investigation, Validation. **Claudio Badini:** Writing - review & editing, Conceptualization, Supervision.

Declaration of competing interest

The authors declare that they have no known competing financial interests or personal relationships that could have appeared to influence the work reported in this paper.

Acknowledgement

This research did not receive any specific grant from funding agencies in the public, commercial, or not-for-profit sectors.

The processed data required to reproduce these findings are available to download from: Padovano, Elisa (2020), "Fused Deposition Modeling and Laser Writing of CF/PA12 composites", Mendeley Data, V2, doi: 10.17632/7y52v52js4.2

References

[1] S.C. Ligon, R. Liska, J. Stampfl, M. Gurr, R. Mülhaupt, Polymers for 3D printing and customized additive manufacturing, Chem. Rev. 117 (2017) 10212–10290, https://doi.org/10.1021/acs.chemrev.7b00074.

[2] X. Wang, M. Jiang, Z. Zhou, J. Gou, D. Hui, 3D printing of polymer matrix composites: a review and prospective, Compos. Part B Eng. 110 (2017) 442–458, https://doi.org/10.1016/j.compositesb.2016.11.034.

[3] O.S. Carneiro, A.F. Silva, R. Gomes, Fused deposition modeling with polypropylene, Mater. Des. 83 (2015) 768–776, https://doi.org/10.1016/j.matdes.2015.06.053.

[4] F. Ning, W. Cong, J. Qiu, J. Wei, S. Wang, Additive manufacturing of carbon fiber reinforced thermoplastic composites using fused deposition modeling, Compos. Part B Eng. 80 (2015) 369–378.

[5] B. Brenken, E. Barocio, A. Favaloro, V. Kunc, R.B. Pipes, Fused filament fabrication of fiber-reinforced polymers: a review, Addit. Manuf. 21 (2018) 1–16, https://doi.org/10.1016/j.addma.2018.01.002.

[6] S.H. Ahn, M. Montero, D. Odell, S. Roundy, P.K. Wright, Anisotropic material properties of fused deposition modeling ABS, Rapid Prototyp. J. 8 (2002) 248–257, https://doi.org/10.1108/13552540210441166.

[7] A. Bellini, S. Güçeri, Mechanical characterization of parts fabricated using fused deposition modeling, Rapid Prototyp. J. 9 (2003) 252–264, https://doi.org/10.1108/13552540310489631.

[8] A.K. Sood, R.K. Ohdar, S.S. Mahapatra, Parametric appraisal of mechanical property of fused deposition modelling processed parts, Mater. Des. 31 (2010) 287–295.

[9] E. Padovano, M. Galfione, P. Concialdi, G. Lucco, C. Badini, Mechanical and thermal behavior of Ultem® 9085 fabricated by fused-deposition modeling, Appl. Sci. 10 (2020) 3170, https://doi.org/10.3390/app10093170.

[10] H.L. Tekinalp, V. Kunc, G.M. Velez-Garcia, C.E. Duty, L.J. Love, A.K. Naskar, C.A. Blue, S. Ozcan, Highly oriented carbon fiber-polymer composites via additive manufacturing, Compos. Sci. Technol. 105 (2014) 144–150, https://doi.org/10.1016/j.compscitech.2014.10.009.

[11] D. Jiang, D.E. Smith, Anisotropic mechanical properties of oriented carbon fiber filled polymer composites produced with fused filament fabrication, Addit. Manuf. 18 (2017) 84–94, https://doi.org/10.1016/j.addma.2017.08.006.

[12] G. Liao, Z. Li, Y. Cheng, D. Xu, D. Zhu, S. Jiang, J. Guo, X. Chen, G. Xu, Y. Zhu, Properties of oriented carbon fiber/polyamide 12 composite parts fabricated by fused deposition modeling, Mater. Des. 139 (2018) 283–292, https://doi.org/10.1016/j.matdes.2017.11.027.

[13] M.L. Shofner, K. Lozano, F.J. Rodríguez-Macías, E.V. Barrera, Nanofiber-reinforced polymers prepared by fused deposition modeling, J. Appl. Polym. Sci. 89 (2003) 3081–3090.

[14] R.T.L. Ferreira, I.C. Amatte, T.A. Dutra, D. Bürger, Experimental characterization and micrography of 3D printed PLA and PLA reinforced with short carbon fibers, Compos. Part B Eng. 124 (2017) 88–100, https://doi.org/10.1016/j.compositesb.2017.05.013.

[15] F. Ning, W. Cong, Y. Hu, H. Wang, Additive manufacturing of carbon fiber-reinforced plastic composites using fused deposition modeling: effects of process parameters on tensile properties, J. Compos. Mater. 51 (2017) 451–462, https://doi.org/10.1177/0021998316646169.

[16] W. Zhang, C. Cotton, J. Sun, D. Heider, B. Gu, B. Sun, T.W. Chou, Interfacial bonding strength of short carbon fiber/acrylonitrile-butadiene-styrene composites fabricated by fused deposition modeling, Compos. Part B Eng. 137 (2018) 51–59, https://doi.org/10.1016/j.compositesb.2017.11.018.

[17] Q. Li, W. Zhao, Y. Li, W. Yang, G. Wang, Flexural properties and fracture behavior of CF/PEEK in orthogonal building orientation by FDM: microstructure and mechanism, Polymers (Basel) 11 (2019)https://doi.org/10.3390/polym11040656.

[18] C. Duty, V. Kunc, B. Compton, B. Post, D. Erdman, R. Smith, R. Lind, P. Lloyd, L. Love, Structure and mechanical behavior of big area additive manufacturing (BAAM) materials, Rapid Prototyp. J. 23 (2017) 181–189, https://doi.org/10.1108/RPJ-12-2015-0183.

[19] J.M. Chacón, M.A. Caminero, E. García-Plaza, P.J. Núñez, Additive manufacturing of PLA structures using fused deposition modelling: effect of process parameters on mechanical properties and their optimal selection, Mater. Des. 124 (2017) 143–157, https://doi.org/10.1016/j.matdes.2017.03.065.

[20] L.G. Blok, M.L. Longana, H. Yu, B.K.S. Woods, An investigation into 3D printing of fibre reinforced thermoplastic composites, Addit. Manuf. 22 (2018) 176–186, https://doi.org/10.1016/j.addma.2018.04.039.

[21] J. Naranjo-Lozada, H. Ahuett-Garza, P. Orta-Castañón, W.M.H. Verbeeten, D. Sáiz-González, Tensile properties and failure behavior of chopped and continuous carbon fiber composites produced by additive manufacturing, Addit. Manuf. 26 (2019) 227–241, https://doi.org/10.1016/j.addma.2018.12.020.

[22] W. Zhang, A.A. Dehghani-Sanij, R.S. Blackburn, Carbon based conductive polymer composites, J. Mater. Sci. 42 (2007) 3408–3418, https://doi.org/10.1007/s10853-007-1688-5.

[23] A. Zecchina, F. Bardelli, S. Bertarione, G. Caputo, P. Castelli, F. Cesano, P. Civera, D. Demarchi, R. Galli, C. Innocenti, D. Carano, A. Veca, Process for producing conductive and/or piezoresistive traces on a polymeric substrate, EP 448 (2) (2012) 383 A1.

[24] F. Cesano, I. Rattalino, D. Demarchi, F. Bardelli, A. Sanginario, A. Gianturco, A. Veca, C. Viazzi, P. Castelli, D. Scarano, A. Zecchina, Structure and properties of metal-free conductive tracks on polyethylene/multiwalled carbon nanotube composites as obtained by laser stimulated percolation, Carbon N. Y. 61 (2013) 63–71, https://doi.org/10.1016/j.carbon.2013.04.066.

[25] M. Liebscher, B. Krause, P. Pötschke, A. Barz, J. Bliedtner, M. Möhwald, A. Letzsch, Achieving electrical conductive tracks by laser treatment of non-conductive polypropylene/polycarbonate blends filled with MWCNTs, Macromol. Mater. Eng. 299 (2014) 869–877, https://doi.org/10.1002/mame.201300377.

[26] G. Colucci, C. Beltrame, M. Giorcelli, A. Veca, C. Badini, A novel approach to obtain conductive tracks on PP/MWCNT nanocomposites by laser printing, RSC Adv. 6 (2016) 28522–28531, https://doi.org/10.1039/c6ra02726a.

[27] A. Caradonna, F. Tagliafierro, A. Veca, C. Badini, Laser printing of conductive tracks with extremely low electrical resistance on polymer–carbon nanotubes composite: an optimization study of laser setup parameters by design of experiment approach, Polym. Eng. Sci. 58 (2018) 1485–1493, https://doi.org/10.1002/pen.24717.

[28] A. Caradonna, C. Badini, E. Padovano, A. Veca, E. De Meo, M. Pietroluongo, Laser treatments for improving electrical conductivity and piezoresistive behavior of

polymer-carbon nanofiller composites, Micromachines 10 (2019)https://doi.org/10.3390/mi10010063.
[29] T.D. Fornes, D.R. Paul, Crystallization behavior of nylon 6 nanocomposites, Polymer (Guildf) 44 (2003) 3945–3961, https://doi.org/10.1016/S0032-3861(03)00344-6.
[30] M. Funabashi, F. Ninomiya, A. Oishi, W. Mizuno, K. Tahira, S. Tanaka, M. Kunioka, Round Robin tests to determine fiber content of carbon fiber-reinforced thermoplastic composites by combustion and thermogravimetry, J. Polym. 2017 (2017) 1–10, https://doi.org/10.1155/2017/4253181.
[31] B. Krause, L. Kroschwald, P. Pötschke, The influence of the blend ratio in PA6/PA66/MWCNT blend composites on the electrical and thermal properties, Polymers (Basel) 11 (2019)https://doi.org/10.3390/polym11010122.
[32] N.G. Karsli, A. Aytac, Tensile and thermomechanical properties of short carbon fiber reinforced polyamide 6 composites, Compos. Part B Eng. 51 (2013) 270–275, https://doi.org/10.1016/j.compositesb.2013.03.023.
[33] F. Ois Dabrowski, S. Bourbigot, R. Delobel, M. Le Bras, Kinetic modelling of the thermal degradation of polyamide-6 nanocomposite, Eur. Polym. J. 36 (2000) 273–284.
[34] J. Li, L. Tong, Z. Fang, A. Gu, Z. Xu, Thermal degradation behavior of multi-walled carbon nanotubes/polyamide 6 composites, Polym. Degrad. Stab. 91 (2006) 2046–2052, https://doi.org/10.1016/j.polymdegradstab. 2006.02.001.
[35] T.L. Dhami, L.M. Manocha, P. Bahl, Oxidation behaviour of pitch based carbon fibers, Carbon N. Y 29 (1991) 51–60.
[36] A.J. Hassani, Z.A. Mohd Ishak, A.R. Mohamed, Preparation and characterization of polyamide 6 nanocomposites using MWCNTs based on bimetallic Co-Mo/MgO catalyst, Express Polym Lett 8 (2014) 177–186, https://doi.org/10.3144/expresspolymlett.2014.21.
[37] C. Dearmitt, Encyclopedia of polymers and composites, Polym. Compos. (2014) https://doi.org/10.1007/978-3-642-37179-0.
[38] E.V. de Toro, J.C. Sobrino, A.M. Martínez, V.M. Eguía, J.A. Pérez, Investigation of a short carbon fibre-reinforced polyamide and comparison of two manufacturing processes: fused deposition modelling (FDM) and polymer injection moulding (PIM), Materials (Basel) 13 (2020) 672, https://doi.org/10.3390/ma13030672.
[39] K.S. Lee, W. Lee, K. Chung, J. Kang, J.R. Youn, Measurement and numerical simulation of three-dimensional fiber orientation states in injection-molded short-fiber-reinforced plastics, J. Appl. Polym. Sci. 88 (2003) 500–509.
[40] B.P. Heller, D.E. Smith, D.A. Jack, Effects of extrudate swell and nozzle geometry on fiber orientation in fused filament fabrication nozzle flow, Addit. Manuf. 12 (2016) 252–264.
[41] E.A. Papon, A. Haque, Tensile properties, void contents, dispersion and fracture behaviour of 3D printed carbon nanofiber reinforced composites, J. Reinf. Plast. Compos. 37 (2018) 381–395, https://doi.org/10.1177/0731684417750477.
[42] E. Padovano, M.E. Bonelli, A. Veca, E. De Meo, C. Badini, Effect of long-term mechanical cycling and laser surface treatment on piezoresistive properties of SEBS-CNTs composites, React. Funct. Polym. 152 (2020)https://doi.org/10.1016/j.reactfunctpolym.2020.104601.
[43] X. Ruan, R. Wang, J. Luo, Y. Yao, T. Liu, Experimental and modeling study of CO2 laser writing induced polyimide carbonization process, Mater. Des. 160 (2018) 1168–1177, https://doi.org/10.1016/j.matdes.2018.10.050.
[44] M. Faes, E. Ferraris, D. Moens, Influence of inter-layer cooling time on the quasi-static properties of ABS components produced via fused deposition modelling, Procedia CIRP 42 (2016) 748–753, https://doi.org/10.1016/j.procir.2016.02.313.
[45] S.J. Leigh, R.J. Bradley, C.P. Purssell, D.R. Billson, D.A. Hutchins, A simple, low-cost conductive composite material for 3D printing of electronic sensors, PLoS One 7 (2012)https://doi.org/10.1371/journal.pone.0049365.
[46] D. Espalin, D.W. Muse, E. MacDonald, R.B. Wicker, 3D printing multifunctionality: structures with electronics, Int. J. Adv. Manuf. Technol. 72 (2014) 963–978, https://doi.org/10.1007/s00170-014-5717-7.
[47] T.H.J. Van Osch, J. Perelaer, A.W.M. De Laat, U.S. Schubert, Inkjet printing of narrow conductive tracks on untreated polymeric substrates, Adv. Mater. 20 (2008) 343–345, https://doi.org/10.1002/adma.200701876.
[48] J. Perelaer, B.J. De Gans, U.S. Schubert, Ink-jet printing and microwave sintering of conductive silver tracks, Adv. Mater. 18 (2006) 2101–2104, https://doi.org/10.1002/adma.200502422.
[49] J. Li, T. Wasley, T.T. Nguyen, V.D. Ta, J.D. Shephard, J. Stringer, P. Smith, E. Esenturk, C. Connaughton, R. Kay, Hybrid additive manufacturing of 3D electronic systems, J. Micromechanics Microengineering 26 (2016)https://doi.org/10.1088/0960-1317/26/10/105005.
[50] S.Y. Wu, C. Yang, W. Hsu, L. Lin, 3D-printed microelectronics for integrated circuitry and passive wireless sensors, Microsystems Nanoeng 1 (2015)https://doi.org/10.1038/micronano.2015.13.
[51] B. Urasinska-Wojcik, N. Chilton, P. Todd, C. Elsworthy, M. Bates, G. Roberts, G.J. Gibbons, Integrated manufacture of polymer and conductive tracks for real-world applications, Addit. Manuf. 29 (2019)https://doi.org/10.1016/j.addma.2019.06.028.
[52] SGL Carbon, SIGRAFIL Short Carbon Fibers Datasheet, Meitingen2020.
[53] X. Yao, C. Luan, D. Zhang, L. Lan, J. Fu, Evaluation of carbon fiber-embedded 3D printed structures for strengthening and structural-health monitoring, Mater. Des. 114 (2017) 424–432, https://doi.org/10.1016/j.matdes.2016.10.078.